

Noise conductance of carbon nanotube transistors

J. Chaste,^{1,2} E. Pallecchi,^{1,2} P. Morfin,^{1,2} G. Fève,^{1,2} T. Kontos,^{1,2} J.-M. Berroir,^{1,2} P. Hakonen,³ and B. Plaçais^{1,2,*}

¹*Ecole Normale Supérieure, Laboratoire Pierre Aigrain, 24 rue Lhomond, 75005 Paris, France*

²*CNRS UMR8551, Laboratoire associé aux universités Pierre et Marie Curie et Denis Diderot, France*

³*Helsinki University of Technology, Low Temperature Laboratory, Puumiehenkuja 2 B, Espoo, P.O. Box 5100, FI-02015 TKK, FINLAND*

(Dated: September 30, 2009)

We report on radio-frequency transmission and noise measurements of high-transconductance carbon nanotube transistors. Gate capacitance C_g , drain conductance g_d , transconductance g_m and current-noise data are analyzed with a ballistic 1-dimensional nano-transistor model where the nanotube channel is described by a quantum capacitance C_q . Current is thermally activated with a transconductance controlled by a bias-dependent electronic temperature. Shot-noise is a thermal noise with a noise conductance g_n different from the drain conductance g_d . The 1-dimensional model gives a simple formula $g_n - g_d = g_m(C_q/2C_g)$ which is verified in the nanotube transistor. Finally we estimate the charge resolution of nanotube devices for applications as fast single-shot electron detectors.

PACS numbers: 73.63.Fg, 72.10.Di, 73.22.f

Carbon nanotubes have long been recognized as model ballistic 1-dimensional (1D) nano-conductors [1] and heavily studied as such since. When used as quantum dots, in the Coulomb blockade or Kondo regimes, nanotubes exhibit quantum noise [2]. Ballistic transport can be observed in metallic wires, signaled by a quantized linear conductance [3] and the vanishing of shot-noise [4, 5]. Applications in both regimes include single electron and field effect transistors (SETs and FETs) [6, 7]. The former are shot-noise limited at finite bias while this is less clear for the latter. In FETs, the diffusive regime has been extensively studied, mostly from DC characteristics [8]. Their ballistic limit, extensively studied theoretically [9], is more difficult to establish as DC current and low-frequency noise of short nanotubes are altered by the effects of the Schottky barrier at the contacts. This difficulty can be overcome at high frequency where capacitive shorting of Schottky barriers allows to reveal intrinsic FET characteristics. Recent transmission measurements at room temperature have confirmed GHz transistor operation and provided accurate RF determinations of gate capacitance C_g and transconductance g_m [10]. In the present work we report on broadband RF transmission and noise measurements at cryogenic temperatures on a representative high-transconductance device. We rely on the direct comparison of RF transconductance and noise to establish, with support of theory, the nano-FET behavior of carbon nanotube transistors.

Top-gated nanotube devices benefit from efficient control of local barriers at moderate gate voltages $V_g \lesssim 1$ V. They have large transconductances $g_m \gtrsim 10 \mu\text{S}$ and gate capacitances can approach the quantum limit $C_g/L_g \lesssim C_q/L_g = 8e^2/hv_F = 0.4 \text{ fF}/\mu\text{m}$ where $v_F \simeq 8 \times 10^5 \text{ m/s}$ is the Fermi velocity and L_g the gate

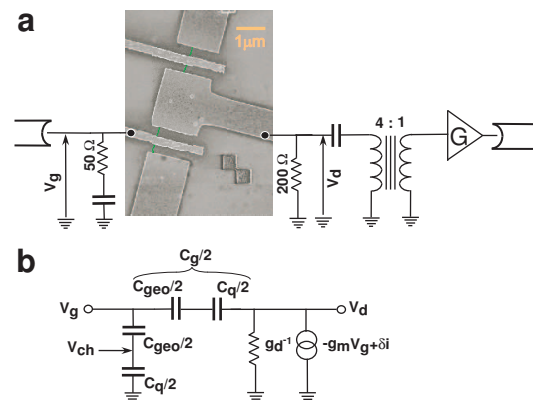


FIG. 1: Double gate nanotube transistor with its measuring scheme (a) and its low frequency electro-chemical equivalent circuit (b). Nanotube diameter is about 2 nm. Transistors parameters are the channel resistance g_d^{-1} , the transconductance g_m , gate capacitance C_g and its geometrical and quantum contributions (C_{geo} and C_q) and the noise current generator δi . In this lumped element description the channel potential, $V_{ch} = V_g \times C_g/C_q$, can be identified with the barrier height $\Phi = -e(V_{ch} + \text{Const.})$.

length. Resulting transit frequencies $\omega_T = g_m/C_g$ approach the ballistic limit, $v_F/2L_g \sim 2\pi \times 200 \text{ GHz}$ for $L_g \lesssim 0.3 \mu\text{m}$. Combination of large ω_T , low current noise S_I and low power consumption favors applications of nano-FETs as charge sensors with a charge resolution $\delta q^* = \sqrt{S_I}/\omega_T \sim 10 \mu\text{e}/\sqrt{\text{Hz}}$ suitable for an emerging subnanosecond quantum single-electronics [11].

As gates are longer than coherence length at high bias and/or high temperature, electronic transport in nano-FETs is classical and thermally activated. At low bath temperatures hot electron effects lead to thermal activation. These are prominent in nanotubes as drain/source reservoirs are constituted by the nanotube itself which has a poor thermal link to the contact which act as ther-

*Electronic address: Bernard.Placais@lpa.ens.fr

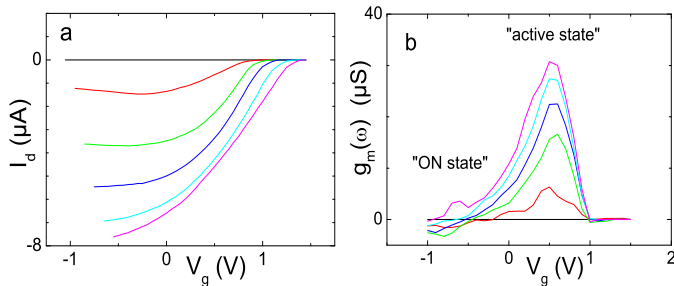


FIG. 2: DC current (a) and transconductance $g_m(\omega)$ (b) as function of gate voltage V_g for a series of equidistant drain voltage values $V_d = -\{0, 0.1, 0.3, 0.5, 0.7, 0.9\}$ V. DC transconductance is qualitatively similar to $g_m(\omega)(V_g)$ within a factor 3 in amplitude. The RF transconductance $g_m(\omega) = \Re[S_{21}(\omega)]/2Z_0$, where Z_0 is the output line impedance is deduced from the transmission $S_{21}(\omega)$ in the 0.2–0.8 GHz band. Transconductance peak at $V_g \sim +0.5$ V define the "active state" of the transistor. The nanotube channel is open at negative gate voltage which is the "ON state" of the transistor.

mal sink. In these conditions current noise writes as a thermal noise

$$S_I = 4g_n k_B T_e \quad (1)$$

proportional to the electronic temperature T_e in the nanotube leads. The prefactor defines a *noise conductance* g_n which is a property of the barrier.

At equilibrium one has the Johnson-Nyquist noise result, $g_n = g_d$, where g_d stands for the real part of the drain admittance. In a multi-terminal active device however, g_n may exceed g_d . This was noticed early in the sixties by van der Ziel who provided an expression of $g_n(V_g, V_d)$ for bulk solid state transistors [12], denoted in the reference as a noise resistance $R_n = g_n/g_m^2$. It was confirmed by experiment shortly after [13]. Noise calculations were later extended to ballistic 2D nano-FETs in Ref.[14]. In electronics, noise conductance effects are accounted for by the introduction of an empirical factor $g_n/g_d \gtrsim 1$ (see review in [15]). In general the determination of g_n requires solving the full 3D or 2D electrostatic problem. As shown below the situation is simpler for ballistic 1D-channels where we obtain simple formula, $g_n - g_d = g_m/2\beta$, that relates the excess noise conductance to transconductance $g_m(V_d, V_g) \equiv \partial I_d / \partial V_g$ via the gate coupling factor $\beta = C_g/C_q \lesssim 1$. As voltage gain $g_m/g_d \sim 1$ and $\beta \lesssim 0.2$ in nanotube transistors, this correction can be of order unity with peak values $g_n \simeq g_m/2\beta \gg g_d$. This is the case for our sample at the $V_g \simeq +0.5$ V transconductance peak in Fig.2-b. This regime will be referred to below as the "active state". At low bias and/or in the transistor "ON state" ($V_g \lesssim 0$ in Fig.2-b), g_m is strongly suppressed so that $g_n \simeq g_d$. The two limiting cases will be considered separately below.

CVD-grown nanotubes are used which give p-channel transistors in the depletion-mode (naturally ON). A

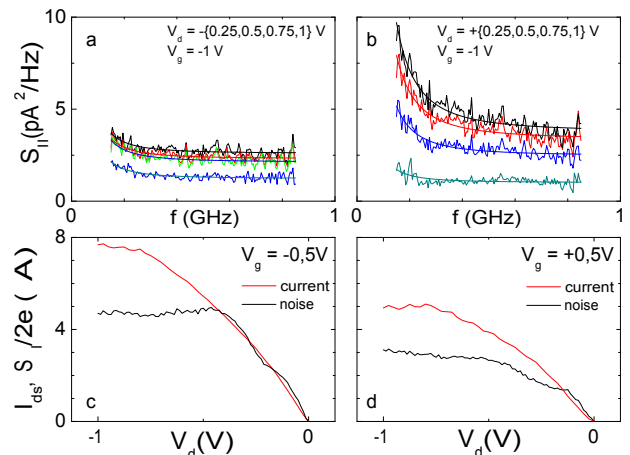


FIG. 3: Noise spectra of carbon nanotube transistors on the ON state at negative (a) and positive (b) bias ($|V_d| = 0.25, 0.5, 0.75, 1$ V). Theoretical fitting by a $A + B/f^2$ law (solid lines) is used to separate shot-noise $S_I = A$ from Lorentzian (B/f^2) noise tails. Bias voltage dependence of shot-noise at negative gate voltage in the ON state (c) and positive gate voltage in the active state (d). DC characteristics are added for direct current to noise comparison.

standard symmetric double gate design is used with $0.3 \mu\text{m}$ gate length as shown in Fig.1 and described in [10, 16]. We measure RF transmission $S_{21}(\omega)$ at room (RT) and low (4K) temperatures from which we deduce both gate capacitance $C_g(\omega)$ and transconductance $g_m(\omega)$ [10]. Cryogenic characteristics of a representative high-transconductance device are given in Fig.2. g_m -data are similar to their RT counterpart besides an increase of $\sim 50\%$ of the peak transconductance. Length dependence gives $C_g/L_g \sim 0.06$ fF/ μm , in agreement with theoretical estimates $C_g/L_g = \beta C_q/L_g \sim 0.08$ fF/ μm taking a geometrical capacitance $C_{geo}/L_g \sim 0.1$ fF/ μm , so that $\beta = C_{geo}/(C_q + C_{geo}) \sim 0.2$. RT carrier mobility, $\mu = g_m L_g^2 / C_q V_d \simeq 0.35 \text{ m}^2 \text{ V}^{-1} \text{ s}^{-1}$, corresponds to a mean-free-path of $v_F m^* \mu / e \sim 0.1 \mu\text{m}$ ($m^* \sim 0.05 m_0$).

Our cryogenic setup, sketched in Fig.1, has a noise temperature of 13.5 K at 4 K in the 0.2–0.8 GHz bandwidth of the experiment. This gives a noise temperature resolution $\lesssim 100$ mK in an averaging time $\gtrsim 1$ s. It includes a 200–50 Ohms matching transformer to enhance current noise resolution to $S_I/2e \lesssim 100$ nA. We use shunting resistors for flat-band response in a bandwidth 0.2–0.8 GHz (Fig.3). This scheme forbids access to reflection coefficient $S_{22}(\omega)$ and prevents measurement of the channel conductance $g_d(\omega)$. Both bias polarities, $V_d = \pm(0 \rightarrow 1)$ V, have been investigated giving similar results with however better noise figures for the negative bias as seen in Figs.3-a and -b. The latter is chosen in the analysis below. The residual low frequency noise is subtracted by spectrum analysis to provide accurate determination of the shot noise intensity up to the maximum

bias in Figs.3-c and -d. We have used symmetric bias conditions for the gate by applying a voltage $\bar{V}_g = V_g + V_d/2$. DC current (Fig.2-a) is obtained after subtraction of the current in the bias resistance, measured at the pinch-off. Complementary DC conductance and transconductance are obtained by numerical differentiation of the $I_d(V_d, V_g)$ data. We observe an enhancement of transconductance at RF, by a factor $g_m(\omega)/g_m(0) \simeq 3$. This effect is generally attributed to capacitive shorting of the Schottky barriers at contacts [17].

Before entering into a detailed analysis of the active FET mode, we consider the ON state ($V_g \leq 0$ in Fig.2) which we analyze by standard Johnson noise thermometry ($g_n = g_d$). In this regime the local gate barrier is smaller than the Schottky barriers at the contact, characterized by an overall transmission $D \sim 0.1$ (deduced from Fig.3-c). In the absence of direct measurement of $g_d(\omega)$ we assume $g_d(\omega) \propto g_m(\omega)$ and take $g_d(\omega) \sim 3g_d(0)$ to estimate the electronic temperature T_e in Fig.4-a. Data correspond to three different bias $V_g = -\{0, 0.25, 0.5\}$ V which have slightly different DC and noise characteristics. They collapse into single line $k_B T_e/e \sim 0.2V_d$ at low bias. This order of magnitude is consistent with a rough estimate of Joule heating associated with the Wiedemann-Franz thermal resistance [18], $k_B T_e/eV_d \sim \sqrt{6D/\pi^2} \sim 0.25$. The line is followed by a saturation at a thermal energy $k_B T_e \lesssim 0.15$ eV comparable with the optical phonon energy. This is a possible consequence of the strong electron-phonon interaction at 1D. However, control experiments using metallic nanotubes are needed to shed more light on the electron-phonon mechanisms [19]. Before discussing results on the active state we present relevant theoretical expectations for the ballistic regime of a 1-dimensional nano-FET.

We model ballistic 1-dim nano-FETs by a classical barrier of energy height Φ , with a transmission $D = 0$ for $E < \Phi$ and $D = 1$ for $E > \Phi$. The current, differential conductance, transconductance of a four-fold degenerate single-band nanotube transistor can be calculated using quantum scattering as [20]

$$I_d = \frac{4e}{h} \int_{\Phi}^{\infty} [f_s(E) - f_d(E)] dE \quad (2)$$

$$g_d = \frac{4e^2}{h} f_s(\Phi + eV_d) \quad (3)$$

$$g_m = \beta \frac{4e^2}{h} [f_s(\Phi) - f_s(\Phi + eV_d)] \quad (4)$$

where $f_s(E) = (1 + \exp[(E - E_F)/k_B T])^{-1}$, and $f_d(E) = f_s(E + eV_d)$ are the Fermi functions at the source and drain reservoirs [21]. From the small-signal electrochemical equivalent circuit of Fig.1 we deduce the gate coupling coefficient $\beta \equiv (1/e)\partial\Phi/\partial V_g = C_g/C_q$. For β and g_d we have disregarded small additional contributions in $\partial\Phi/\partial V_d$. Otherwise we fully take into account the drain voltage dependence of barrier in the $\Phi(V_d)$ dependence of g_m and g_d in Eqs.(3) and (4).

From Eq.(4) we estimate the uppermost value of

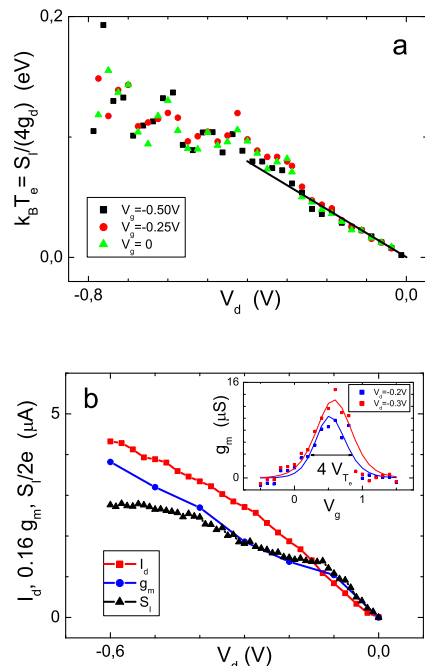


FIG. 4: a) Noise temperature in the ON state ($V_g \leq 0$), deduced from shot-noise and RF differential conductance $g_d(\omega) \sim 3g_d(0)$. Solid curve is the line $k_B T_e/e = 0.2V_d$. b) Active state with $V_g \sim +0.5$ V: RF noise $S_I(\omega)$ and transconductance $g_n(\omega)$ together with DC current I_d as function of bias voltage V_d (main Frame). RF transconductance $g_m(V_g)$ at $V_d = -0.2$ V (resp. -0.3 V) (inset). Theoretical adjustment with Eq.(4), with $\beta^* \frac{8e^2}{h} = 30 \mu\text{S}$ (taking $\beta^* = 0.5\beta = 0.1$) and a gate potential shift of 0.6 V (resp. 0.73 V), gives $V_{T_e} = k_B T_e/(\beta e) = 0.13$ V (resp. 0.16 V) which corresponds to $k_B T_e = 26$ meV (resp. 32 meV).

transconductance, $g_m = 8\beta e^2/h \times f_s(0) = 62 \mu\text{S}$ for degenerate leads with $f_s(0) = 1$, in our double gate transistor ($\beta = 0.2$). The measured value, $g_m \simeq 30 \mu\text{S}$ in Fig.2-b, is only a factor two below this upper limit. However, this large value was obtained at an already large bias $|V_d| \gtrsim 0.5$ V for which contributions from additional sub-bands can be expected. Therefore, we shall restrict our theoretical analysis to the $|V_d| \lesssim 0.3$ V data, as reproduced in the inset of Fig.4-b. Theoretical fitting with Eq.(4), taking $0 \lesssim E_F \ll k_B T_e$ as a hot electron approximation, gives an exponential gate voltage dependence with a characteristic voltage, $V_{T_e} = k_B T_e/e\beta \simeq 0.16$ V (at $V_d = -0.3$ V) which corresponds to a thermal energy $k_B T_e \simeq 32$ meV. This large value, close to RT conditions, confirms the hot electron scenario already observed in the ON state. It is also consistent with the weak temperature dependence of transconductance between RT and 4 K. A scaling factor 0.5 has been applied to theoretical lines to account for residual scattering due to finite gate length.

Noise can be calculated using the same formalism [20]:

$$S_I = 2 \frac{4e^2}{h} \int_{\Phi}^{\infty} [f_s(1 - f_s) + f_d(1 - f_d)] dE \quad (5)$$

$$= 2k_B T \frac{4e^2}{h} [f_s(\Phi) + f_s(\Phi + eV_d)] \quad (6)$$

Eq.(5) incorporates only the thermal noise and disregards quantum partition noise as $D(1 - D) = 0$ in the classical ballistic limit. Using Eqs.(3) and (4), we get from Eq.(6) the formula for the noise conductance :

$$g_n = S_I/4k_B T_e = g_d + g_m/2\beta \quad (7)$$

Eq.(7) is the central result of our paper. It predicts a strong deviation from Johnson-Nyquist noise in bias conditions where voltage gain $g_m/g_d \gtrsim \beta$ is significant. This situation prevails in the "active state" at large enough bias where $g_n \simeq g_m/2\beta \simeq 33 \mu\text{S}$ ($V_g = +0.5 \text{ V}$, $V_d = -0.3 \text{ V}$) is much larger than $g_d(0) \sim 5 \mu\text{S}$, in agreement with the theoretical estimate $g_n/g_d \gtrsim 4$. In this case Eq.(6) reduces to $S_I/2e \simeq g_m \times V_{T_e}$, where V_{T_e} has been deduced from the gate-voltage dependence of g_m (see inset of Fig.4). An experimental test, which relies on parameter-free comparison of the two characteristic currents $S_I/2e$ and $g_m V_{T_e}$, is shown in Fig.4-b where the scaling factor $V_{T_e} = 0.16 \text{ V}$ has been taken that corresponds to the electronic temperature $k_B T_e \simeq 32 \text{ meV}$ at the working bias $V_d = -0.3 \text{ V}$. We regard this parameter-free agreement, and the semi-quantitative prediction of transconductance, as strong support of the above 1-dim nano-FET model. When complemented by direct measurement of $g_d(\omega)$, further investigation should allow to cover the full bias range so as to study the crossover case $g_m/2\beta \sim g_d$ in greater detail.

Taking into account the DC current, one can alternatively express thermal noise as $S_I = 2eI_d \mathcal{F}$, defining of a Fano-like factor $\mathcal{F} = 2g_n k_B T_e / eI_d$. With $f_s(E) \simeq \exp(-E/kT)$ in the non-degenerate case, current and noise expressions (2) and (5) simplify at low bias to yield $\mathcal{F} = \coth(eV_d/2k_B T_e)$. In the absence of detailed account of the energy distribution in nanotube transistor leads, one can rely on energy conservation limit, $2k_B T_e / eV_d \lesssim 1$, to estimate the Fano factor range $\mathcal{F} \sim 1-1.3$. This behavior is indeed observed for $V_d \lesssim 0.1 \text{ V}$ in Fig.4-b. At higher bias, Fermi suppression

of shot-noise due to drain lowering of the barrier is expected and observed with $\mathcal{F} < 1$ corresponding to a sub-linear increase of T_e with V_d . At large bias, $|V_d| \gtrsim 0.3 \text{ V}$, a second noise step is seen in the active state, also observed in the ON state (Fig.3-c), that one may attribute to the onset of second-subband conduction. Note that most of the features observed in the noise data are absent in DC transport characteristics, which emphasizes once again the richness of a noise analysis.

Finally, we can estimate from our measurements the charge resolution of carbon nanotube transistors. The best signal to noise conditions for charge detection correspond to the 0.3 V bias range with a moderate dissipative power ($I_d V_d \sim 1 \mu\text{W}$). From $C_g \lesssim 40 \text{ aF}$ (RT measurements [10]), $g_m \gtrsim 15 \mu\text{S}$ and $S_I/2e \lesssim 2 \mu\text{A}$, we estimate the charge sensitivity $\delta q_{rms} = \sqrt{S_I}/\omega_T \sim 13 \mu\text{e}/\sqrt{\text{Hz}}$ for our double gate device which corresponds to an *rms* charge resolution of 0.4 electron in the 0.8 GHz bandwidth of our set-up. Within a factor five of the best resolution achieved in SETs [6], this value can still be optimized by reducing gate length below $0.1 \mu\text{m}$ for a fully ballistic regime in a single gate device. The smaller sensitivity of the present CNT-FETs, and more generally of nano-FETs, with respect to SETs is however balanced by a much larger bandwidth (0.8 GHz here against 0.08 GHz in [6]).

In conclusion, we have performed comprehensive RF measurements of transconductance and shot noise in quasi-ballistic nanotube transistors. Our data, in particular the noise conductance, are consistent with a 1-dim ballistic nano-FET model. Finally we have benchmarked nanotube FETs against nanotube SETs as fast single electron detectors.

Acknowledgments

Authors acknowledge fruitful discussions with G. Dambrine, V. Derycke, P. Dollfus, C. Glattli, H. Happy and M. Sanquer. The research has been supported by french ANR under contracts ANR-2005-055-HF-CNT, ANR-05-NANO-010-01-NL-SBPC, and EU-STREP project CARDEQ under contract IST-FP6-011285.

-
- [1] S.J. Tans, A.R.M. Verschueren, and C. Dekker, *Nature* **393**, 49 (1998).
 [2] T. Delattre, C. Feuillet-Palma, L. G. Herrmann, P. Morfin, J.-M. Berroir, G. Fve, B. Plaçais, D. C. Glattli, M.-S. Choi, C. Mora, and T. Kontos, *Nature Phys.* **5**, 208 (2009).
 [3] W. Liang et al., *Nature (London)* **411**, 665 (2001).
 [4] F. Wu, P. Queipo, A. Nasibulin, T. Tsuneta, T.H. Wang, E. Kauppinen and P. J. Hakonen, *Phys. Rev. Lett.* **99**,

- 156803 (2007).
 [5] L.G. Herrmann, T. Delattre, P. Morfin, J.-M. Berroir, B. Plaçais, D.C. Glattli, T. Kontos *Phys. Rev. Lett.* **99**, 156804 (2007).
 [6] S. E. S. Andresen, F. Wu, R. Danneau, D. Gunnarsson and P. J. Hakonen, *J. Appl. Phys* **104**, 033715 (2008).
 [7] F. Wu, T. Tsuneta, R. Tarkiainen, D. Gunnarsson, T.H. Wang, and P.J. Hakonen, *Phys. Rev. B* **75**, 125419 (2007).

- [8] X. Zhou, J.-Y. Park, S. Huang, J. Liu and P. L. McEuen, *Phys. Rev. Lett.* **95**, 146805 (2005).
- [9] D. Akinwande, J. Liang, S. Chong, Y. Nishi, H.-S. Wong, *J. Appl. Phys* **104**, 124514 (2008).
- [10] J. Chaste, L. Lechner, P. Morfin, G. Fve, T. Kontos, J.-M. Berroir, D. C. Glattli, H. Happy, P. Hakonen, B. Plaçais, *Nano Lett.* **8**, 525 (2008)
- [11] G. Fève, A. Mahé, B. Plaçais, J.-M. Berroir, T. Kontos, A. Cavanna, Y. Jin, B. Etienne and D. C. Glattli *Science* **316**, 1169 (2007).
- [12] A. van der Ziel, *Proc. IRE* **50**, 1808 (1962).
- [13] W.C. Bruscke, *Proc. IEEE* **51**, 378 (1963).
- [14] Y. Naveh, A.N. Korotkov, and K.K. Likharev, *Phys. Rev. B* **60**, 2169 (1999).
- [15] Jindal RP, *IEEE Trans. on Electron Devices* **53**, 9 (2006).
- [16] J. Chaste, thesis, Université Pierre et Marie Curie, Paris, 2009; online access at (<http://tel.ccsd.cnrs.fr>), tel-00420915, v1.
- [17] S. Li, Z. Yu, S-F. Yen, W. C. Tang, and P-J. Burke *Nano Lett.* **4**, 753 (2004)
- [18] A. Kumar, L. Saminadayar, D. C. Glattli, Y. Jin and B. Etienne, *Phys. Rev. Lett.* **76**, 2778 (1996).
- [19] F. Wu, P. Virtanen, J.K. Viljas, S. Andresen, T. Heikkila, B. Placais, and P.J. Hakonen, arXiv (2009).
- [20] Y.M. Blanter, M. Büttiker, *Phys. Rep.* **336**, 1 (2000)
- [21] In the theoretical description we assume that channel carriers are electrons; all discussion and equations can be applicable to the actual p-channel counterpart with appropriate substitution of parameters and reversal of polarity of the applied voltages.